ALMA Memo 403
Fast Switching Phase Correction Revisited for 64 12 m Antennas

M.A. Holdaway
National Radio Astronomy Observatory
949 N. Cherry Ave.
Tucson, AZ 85721-0655
email: mholdawa@nrao.edu

December 18, 2001

Abstract

Fast switching phase calibration has not been investigated for the ALMA telescope since ALMA has been defined as 64 12 m antennas. Furthermore, the logic chain which picked the optimal calibrator in past investigations was approximate. In order to better understand the requirements which are placed on the current ALMA design by fast switching, we have rewritten the fast switching simulation code in AIPS++, including a more complete optimization with fewer assumptions, using updated sensitivity, antenna slewing, and atmospheric information.

We find that when the observing frequency is matched to the phase stability (ie, high frequency observations are always carried out during the most stable phase conditions), the Chajnantor site is good enough to permit fast switching observations of the expected frequency range (ie 30 to 950 GHz) to succeed with high efficiency. Typical observing efficiencies, including both time lost to the phase calibration cycle and decorrelation losses, range between 0.80 and 0.90 for sources above 45 deg elevation angles. The observing efficiency decays very gently at lower elevation angles, with a typical efficiency of 0.70 at 20 deg elevation.

The extra sensitivity provided by 64 12 m antennas does not help as much as might be expected with fast switching because the time spent integrating on the calibrator is very small compared to the entire cycle and is a moderately small portion of the calibration phase of the cycle. The 1.5 s delay due to changing frequencies is pretty well matched to the slew times for typical objects. The slew profiles provided by Vertex are sufficient.

The residual phase errors resulting from fast switching will cause baseline-dependent decorrelation. Some minor algorithmic work should proceed on fixing this decorrelation. It seems likely that the phase information gleaned from observing the calibrator will be sufficient to accurately estimate the decorrelation correction on a per baseline basis.

1 Introduction

In spite of the excellent atmospheric conditions documented above the Chajnantor site (Radford, 2001), the ALMA telescope will usually require some form of advanced phase compensation for observations in array configurations larger than about 100 m.

The atmosphere permits phase stable zenith observations with 20 deg RMS fluctuations or better on 300 m baselines at 95 GHz half the time. At 300 GHz, the atmosphere permits phase stable (ie, 20 deg RMS) observations on 300 m baselines only about 13% of the time. The better the atmospheric stability, the smaller the residual phase error due to fast switching. Hence, fast switching for demanding high frequency observations will work better during the most phase stable atmospheric conditions. This leaves the moderate and poor phase stability conditions for the low frequency projects, and it is likely that *all* ALMA observations with baselines greater than about 100 m will require advanced phase compensation. (Fast switching will not be very effective for baselines shorter than about 100 m, as this is approximately the effective switching scale $vt/2 + d$ at which the phase structure function saturates when fast switching. Shorter baselines could be improved by fast switching using much shorter cycle times, but the observing efficiency would suffer greatly.) The two main competitors for the advanced phase compensation method are radiometric phase correction and fast switching phase calibration. It is possible that both would be used, either together or separately for different types of conditions and observations.

Logistically, radiometric phase correction is preferred over fast switching. Radiometric phase correction is passive, and requires much less time lost off the target source than fast switching. Additionally, fast switching may cause maintenance and power problems, though the prototype designs have taken these issues into consideration, and in principle deal with them effectively.

Success in the various attempts at radiometric phase correction has been very encouraging, but radiometric correction with the accuracy which ALMA demands has been elusive. More advanced experiments are ongoing, and it seems likely that radiometric correction will play a major role in ALMA observations. On the other hand, a full understanding of how to optimize the radiometric correction will probably be developed over the first several years of ALMA observations at the Chajnantor site, and there is no guarantee that it will work with the required accuracy. So even though fast switching is at a logistical disadvantage, it is likely that fast switching will play an important role in the ALMA telescope as well.

So, we present here a new analysis of the fast switching process in the light of our more precise understanding of the ALMA telescope.

2 Features of the Fast Switching Analysis

This round of fast switching phase calibration simulations is different from previous work in this area in a number of key ways:

- **The new analysis of fast switching phase calibration is performed with software written at the glish level of AIPS++.** As AIPS++/glish is a superior computing environment for dealing with complex problems, we have taken the opportunity to upgrade the software which calculates the efficiency and effectiveness of fast switching phase calibration. Optimizing fast switching is a detailed endeavor: we need to observe the calibrator with sufficient SNR to scale the phase solutions to the target frequency, and then go back to the target source and integrate as long as the atmosphere will permit us to. By integrating for a long time, we increase the duty cycle, and hence the efficiency. However, if we integrate too long, decorrelation due to increased phase noise will lower the overall efficiency. So, matters such as the accuracy of the calibrator gain solutions, the residual phase errors on the target source, and the duty cycle, are all parameters to be tweaked with the goal of optimizing the overall observing efficiency. While it is not simple, it is readily doable in AIPS++. The new software is sufficiently different from the old fast switching software in its approach and optimization philosophy that comparisons with the results from the old software are not particularly meaningful: the comparison would mainly reflect the change in the approach.

- **The antenna slewing speed is taken from the Vertex calculations.** Vertex, one of the contractors for the prototype antennas, has done detailed dynamical calculations of fast slewing which does not excite antenna resonances (Vertex PDR, 2000). The two calculations are for 1.5 and 4.0 deg slews in both azimuth and elevation. For our fast switching calculations, we need to estimate the slew time to get to a source an arbitrary distance away. We achieve this estimate by making an empirical model in which the slew is broken into a start-up, a nearly constant velocity slew, and a slow-down. The start-up, slow-down, and constant velocity are determined as a function of slew distance by fitting to the 1.5 deg and 4.0 deg slewing profiles (this will break down for slews much larger than 4.0 deg where the maximum slew velocity will be exceeded, but our calibrator sources are typically only a degree or two away from the target source). The slew time as a function of source distance is diplays graphically in Figure 1, and the details of the model are indicated below:

$$\begin{aligned}
t_{az} &= t_{az}^{start}(\theta_{az}) + \theta_{az}/slew_{az}(\theta_{az}) + t_{az}^{stop}(\theta_{az}) && (1)\\
t_{el} &= t_{el}^{start}(\theta_{el}) + \theta_{el}/slew_{el}(\theta_{el}) + t_{el}^{stop}(\theta_{el}) && (2)\\
t_{az}^{start}(\theta_{az}) &= 0.152 + 0.052\theta_{az} && (3)\\
t_{az}^{stop}(\theta_{az}) &= 0.430 + 0.080\theta_{az} && (4)\\
slew_{az}(\theta_{az}) &= 2.0 + .70\theta_{az} && (5)\\
t_{el}^{start}(\theta_{el}) &= 0.254 + 0.044\theta_{el} && (6)\\
t_{el}^{stop}(\theta_{el}) &= 0.414 + 0.044\theta_{el} && (7)\\
slew_{el}(\theta_{el}) &= 1.724 + .224\theta_{el} && (8)\\
& && (9)
\end{aligned}$$

- **A frequency set up time of 1.5 s is used.** As we are planning to perform the fast switching at 90 GHz, and the target frequency will be anywhere between 30 and 950 GHz, a slew of less than 1.5 s will have some dead time for frequency setup before observations can begin. When the target frequency is between 30 and 115 GHz, we may very well perform the fast switching phase observations at the target frequency. As the on-calibrator integration time is very small at these frequencies, modest differences in sensitivity among the potential calibration frequencies will not change the calculations significantly. Also, as the slew times tend to be about 1.5 s, the absence of the 1.5 s frequency change time will not greatly change the calculations either.

- **90 GHz source counts** are still estimated from Holdaway, Owen, and Rupen (1994). These are now encapsulated in the `sourcecountsim` tool in glish.

- **Atmospheric opacity** is scaled from the measured opacity at 225 GHz to the calibration frequency via Pardo *et. al.*'s new ATM code. For simplicity in this analysis, we consider a

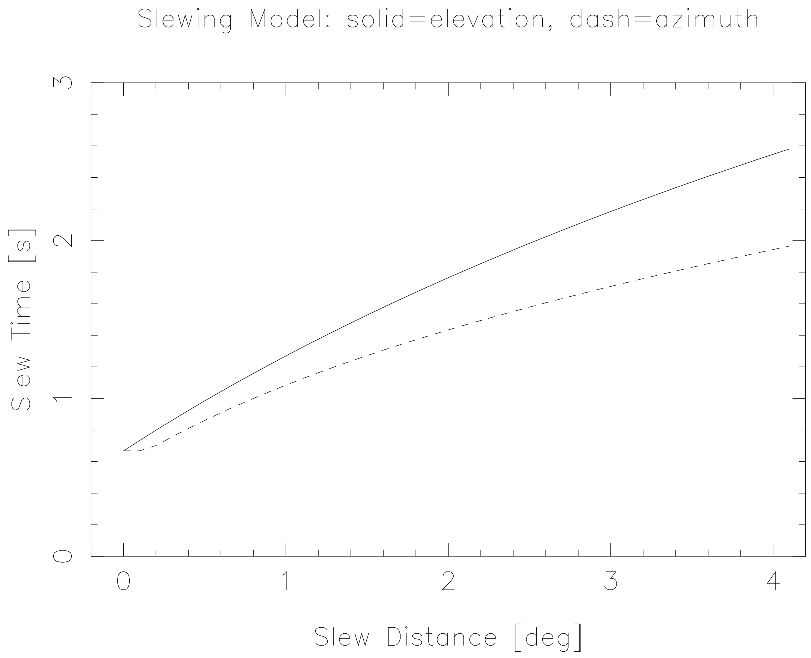

Figure 1: Modeled slew times for azimuth and elevation slews.

single frequency somewhere near each band center: 37 GHz, 81 GHz, 113 GHz, 157 GHz, 209 GHz, 271 GHz, 355 GHz, 415 GHz, 665 GHz, and 868 GHz.

- **Optimally, these calculations would be integrated with dynamic scheduling simulations**, so that a realistic variety of source elevations and target frequencies would be fit into the varying atmospheric conditions. This will be planned for the future, as we are also investigating simulations of dynamic scheduling.

- **The ALMA system definition** includes 64 12 m antennas and system noise consistent with Butler and Wooten (1999).

- **Required phase solution accuracy**, together with the system sensitivity and the calibrator source strength, determines the integration time on the calibrator source. Since we are performing the phase solution with a 90 GHz observation and then scaling the solution up to another frequency, the solution accuracy must be improved by the ratio of the frequencies. Also, the solution accuracy interacts with the atmospheric conditions. For example, it makes little sense to spend lots of time integrating on the calibrator to get a very accurate phase solution when the atmosphere is horrible; you'd much rather spend less time and get a worse solution (but which was still better than the atmospheric phase errors), permitting a shorter cycle time. The contrary situation would occur if the atmosphere were very good and the residual phase errors were dominated by the errors in the gain solution. As a rule of thumb, we seek to put the gain solution errors at 33% of the atmsopheric phase errors over the calibration cycle, so in quadrature they will be a small contribution (5%). These gain errors are due to thermal noise on the calibrator and will be randomized every calibration cycle, so they should not be a limiting factor in observations.

- **Height of the atmospheric turbulence** is taken to be 500 m, as per Robsen *et. al.* (2001) and Delgado *et. al.* (2001).

- **Velocity of the turbulent layer** is taken to be 12 m/s, as Delgado finds the velocity aloft of the turbulent water vapor to be about twice the ground speed, and the median ground speed is 6 m/s.

- **Observing Efficiency:** as mentioned above, there are two sources of inefficiency in fast switching phase calibration: time losses due to the duty cycle, and decorrelation losses due to the residual phase errors. An effciiency factor of

  $$\eta_t = \sqrt{t_{target}/t_{cycle}} \tag{10}$$

  results from the duty cycle, or time lost by observing the calibrator and slewing. In our simulations, the optimal switching strategy favors longer cycle times in which a very large fraction of the time is spent on the target source, resulting in a duty efficiency typically between 0.92 and 0.96. The RMS residual phase error σ_ϕ (in radians) results in a decorrelation efficiency of

  $$\eta_\phi = e^{-\sigma_\phi^2/2}. \tag{11}$$

  This typically ends up being a factor ranging from 0.90 to 0.95. We gauge the success of the fast switching technique as the sensitivity of a fast switching calibrated observation relative to an observation under a turbulence-free atmosphere which requires no calibration at all, and is given by the product of the two efficiencies $\eta_t \eta_\phi$. The overall efficiency ends up being between 0.80 and 0.90 for a realistic distribution of observing conditions and target frequencies.

  The opacity is not considered in calculating the observing efficiency at this time (see below).

- **The observing frequency is matched to the phase stability.** We assumed that the highest frequency observations will take place during the times with the lowest atmospheric phase fluctuations. The fraction of time we assume will be spent observing at each frequency along with the matched atmospheric stability and opacity is presented in Table 1. The opacity is considered only as a dependent variable, in that the median opacity for each bin of ranked phase fluctuations was used, but we have not picked the observing frequency based on opacity. Since the opacity and the phase stability are only moderately correlated, there will be some times of very good phase stability with poor opacity, and vice versa. Including the opacity will have a large effect on the efficiency (ie, at sub-millimeter wavelengths, the efficiency will go way down because the sub-millimeter opacity will rarely be less than 0.5). Including the opacity will move around some of the conditions and observing frequencies; for example, if the phase stability is excellent but the opacity is rather poor, the conditions are not acceptable for sub-millimeter observing, and a lower frequency project will get better phase conditions than expected. Similarly, there will be conditions of low opacity and somewhat worse phase stability that will end up being used for high frequency observations. In the end, including opacity data in a fast switching analysis will result in somewhat larger phase errors for the high frequency observations and somewhat smaller phase errors for the low frequency observations.

Frequency $[GHz]$	Fraction Observed	σ_ϕ [deg] at 11.2 GHz	τ at 225 GHz
37	0.10	12.29	0.1752
81	0.10	7.63	0.1576
113	0.10	5.25	0.1558
157	0.10	3.84	0.1378
209	0.12	2.80	0.1226
271	0.12	2.02	0.0994
355	0.12	1.44	0.0763
415	0.12	0.98	0.0541
650	0.12	0.57	0.0378

Table 1: The fraction of the time we assume will be spent observing in each frequency band along with the median atmospheric phase stability (corrected to zenith observing) and atmospheric opacity.

The next step is to perform a full analysis of fast switching within the context of dynamic scheduling, choosing the observing project based on the observing frequency, the current phase stability, and the current opacity. This work is planned for the near future.

3 Correction for Decorrelation

The decorrelation caused by the residual phase errors will result in baseline dependent amplitude gain errors and must be corrected. For very short baselines, there will be very little decorrelation. For baselines greater than the effective switching scale $vt/2 + d$ (ie, the atmospheric velocity times the cycle time over two, plus the distance between the lines of site to the target and calibrator sources at the typical elevation of the turbulent water vapor; see Holdaway (1992) for more information), the decorrelation will be approximately constant, determined by the phase structure function at this scale. For shorter baselines, the decorrelation will be given by the phase structure function evaluated at that baseline. An approximate solution to this problem would be to calculate the coherence for each baseline given the phase structure function as determined by an independent device such as a site testing interferometer. Then, the visibilities would be corrected on a baseline by baseline basis, dividing by the coherence. The visibility weights would also need to be multiplied by the coherence squared to reflect the loss in sensitivity.

However, the phase structure function as determined locally will not generally be applicable over the entire array (Holdaway, Matsushita, and Saito (1997). An alternative would be to determine the coherence amplitude corrections from the fast switching calibration measurements themselves. The quantity $vt/2 + d$ will be dominated by the time term. In our computations, bringing the turbulent height down to 500 m makes d smaller, and increasing the cycle time to increase the duty efficiency makes the $vt/2$ term larger. Hence, the phase fluctuations at the position of the calibrator source will be very similar to the phase fluctuations at the position of the target source, but the times will be different. Hence, we should be able to use the solution time series on the calibrator source to estimate the effect of decorrelation on the target source visibilities.

4 Results

The basic results for our fast switching simulations are shown in Table 2. When we match the target frequency to the phase stability conditions (ie, observe the highest frequency projects during the conditions of best phase stability), the efficiency of fast switching observations is essentially independent of frequency. This means that the distribution of phase conditions and the distribution of observing frequencies are well matched. In addition, fast switching degrades in a "mushy" manner (see the discussion of degradation with elevation below). Another way of stating this is that all the observations are doable, but none will ever be performed in outstanding conditions. If the conditions are outstanding at the observing frequency, the dynamic scheduling system will probably postpone the current project and schedule a more demanding, higher frequency project.

Fast switching decays rather gently with respect to changes in elevation angle. Low elevation observing conspires to make fast switching difficult: the distance between the lines of site to target and calibrator increases, the phase fluctuations increase, and the sensitivity of the system decreases. Earlier, there was some concern that fast switching may not work at very high elevation angles due to the increase in slew times when making azimuthal slews to and from calibrators. However, as noted above, there are many dimensions of this problem to play with. When the atmosphere starts falling apart at low elevation angles, we can go to a shorter duty cycle, and we can spend less time on the calibrator, or observe a closer, fainter calibrator, as the increased atmospheric phase errors do not require such accurate phase solutions. These interrelated degrees of freedom in the fast switching system make fast switching kind of "mushy". The mean efficiency, averaged over all frequency-matched phase conditions, is shown over a range between 20 and 80 degrees elevation in Table 4. Between an elevation angle of 80 degrees and 20 degrees, the efficiency of fast switching drops by only 17%. Compelling experiments at extreme declinations which must be observed at low elevation angles could experience higher efficiency fast switching by being elevated to improved atmospheric conditions which would otherwise be appropriate to higher frequency observations.

One surprising result is that the increase in antennas from 40 to 64 and the increase in diameter from 8 to 12 m has had very little impact on the effectiveness of fast switching. This is understood in that the time it takes to detect a calibrator with sufficient SNR to extrapolate from 90 GHz to the target frequency is very small indeed, typically 0.05 s at 40 GHz and 0.5 s for 650 GHz. This detection time is much smaller than the time it takes to slew to and from the calibrator. It might seem that with such tiny detection times, it might be more efficient to spend more time on a closer, weaker source. However, not much time is gained in doing so as there is a frequency switching penalty of 1.5 s so no time is saved in going to a closer calibrator, and the d term in $vt/2 + d$ is already tiny compared to the $vt/2$ term.

When including the duty cycle in the efficiency, the results of these calculations push us towards longer cycle times than had previously been envisioned. ALMA Memo 174 (Holdaway, 1997) estimated the total number of switching cycles that would be required for the ALMA antennas. A major variable in that work was what the required residual phase error would be. For example, a factor of 6 times more switching cycles were required to achieve 20 degree residual phase fluctuations than to achieve 45 degree phase fluctuations. The current analysis bypasses that issue and just seeks to find the switching strategy which preserves the most sensitivity. Performing the exact same analysis (ie, the same fraction of time goes to each frequency band as was assumed in Memo 174) results in 25 million switching cycles due to fast switching phase calibration through a 30 year lifetime of the ALMA telescope. Including band 10 (850 GHz, which was not included in this analysis), we will require more switching cycles.

5 Dispersive Phase

At millimeter wavelengths, far from strong and wide atmospheric absorption features, the wet and dry delays are very nearly non-dispersive. However, in the sub-millimeter windows, the water absorption lines are always nearby and there is a significant dispersive phase. In earlier memos, we warned about the possibility of a dispersive component to the phase spoiling the effectiveness of fast switching at sub-millimeter wavelengths. This issue has been investigated quantitatively by Holdaway and Pardo (2001, in preparation). In summary, there is a phase term due to the dispersive phase which is not compensated for by the low frequency calibration in fast switching. This extra residual phase increases with baseline length, with the RMS atmospheric phase fluctuations, and at the low transmission edges of the sub-millimeter transmission windows. It seems likely that the dispersive phase will not adversely affect most ALMA observations, but for some observations (long baselines, marginal phase stability, at frequencies near the edge of the transmission windows) the residual phase errors may be dominated by the dispersive phase, especially if there are significant dry phase fluctuations as well. We do not account for the dispersive phase in the calculations presented here, but only warn that they may further reduce the observing efficiency for the sub-millimeter windows.

6 Acknowledgments

We thank Juan Pardo for letting us use the newest version of his ATM program to calculate the wet and dry terms of the atmospheric opacity at 30 and 90 GHz above the ALMA site. Also, the ALMA Imaging and Calibration group (most notably Simon Radford, Al Wootten, Bryan Butler, and Jeff Mangum) made many helpful comments

References

Butler, B. and A Wooten, ALMA Memo 276, "ALMA Sensitivity, Supra-THz Windows and 20 km Baselines", 1999.

Delgado, Guillermo, and Lars-Ake Nyman, ALMA Memo 363, "Velocity of the Effective Turbulence Layer at Chajnantor Estimated From 183 GHz Measurements", 2001.

Holdaway, M.A., ALMA Memo 84, "Possible Phase Calibration Schemes for the MMA", 1992.

Holdaway, M.A., ALMA Memo 174, "How Many Fast Switching Cycles Will the MMA Make in its Lifetime?", 1997.

ν [GHz]	t_{cal} [s]	t_{slew} [s]	S_{cal} [Jy]	distance [deg]	$vt/2+d$ [m]	σ_ϕ [deg]	coherence eff.	duty eff.	total eff.
80 deg elevation									
37	0.045	1.31	0.037	0.66	189	18.0	0.952	0.953	0.907
81	0.095	1.39	0.057	0.84	155	21.1	0.934	0.942	0.880
113	0.110	1.39	0.069	0.77	122	25.5	0.906	0.925	0.838
157	0.144	1.49	0.088	0.96	135	23.0	0.923	0.925	0.853
209	0.198	1.52	0.099	0.96	155	21.4	0.933	0.925	0.863
271	0.202	1.60	0.126	1.11	144	22.2	0.928	0.925	0.858
355	0.297	1.69	0.136	1.21	154	22.4	0.926	0.925	0.857
415	0.366	1.71	0.143	1.30	172	20.8	0.936	0.925	0.866
650	0.459	1.84	0.201	1.47	161	23.0	0.923	0.925	0.853
60 deg elevation									
37	0.018	1.07	0.061	0.65	186	19.0	0.947	0.953	0.902
81	0.047	1.19	0.083	0.80	144	21.5	0.932	0.925	0.862
113	0.062	1.19	0.088	0.83	118	26.7	0.897	0.925	0.830
157	0.095	1.26	0.109	0.94	134	24.4	0.913	0.925	0.845
209	0.118	1.32	0.131	1.05	139	21.4	0.933	0.925	0.863
271	0.167	1.34	0.141	1.11	140	23.3	0.921	0.925	0.852
355	0.218	1.40	0.164	1.22	143	22.8	0.924	0.925	0.855
415	0.266	1.45	0.174	1.30	164	21.6	0.931	0.942	0.877
650	0.376	1.54	0.229	1.53	151	23.6	0.919	0.925	0.850
45 deg elevation									
37	0.030	1.00	0.051	0.61	172	20.1	0.940	0.942	0.886
81	0.050	1.10	0.082	0.80	143	23.7	0.918	0.925	0.849
113	0.061	1.08	0.078	0.76	109	28.2	0.886	0.894	0.792
157	0.079	1.18	0.110	0.96	136	27.3	0.893	0.925	0.826
209	0.115	1.23	0.137	1.09	143	24.1	0.915	0.925	0.847
271	0.125	1.23	0.156	1.08	144	26.2	0.901	0.925	0.833
355	0.195	1.29	0.167	1.20	145	25.5	0.906	0.925	0.838
415	0.211	1.40	0.199	1.48	152	22.8	0.924	0.925	0.855
650	0.359	1.42	0.232	1.51	147	25.7	0.904	0.925	0.836

Table 2: Fast switching results: by matching the observing frequency to the atmospheric phase conditions and doing 400 Monte Carlo simulations of 90 GHz calibrator fields consistent with 90 GHz source counts, we optimize the switching strategy for each simulated observation and report the median efficiency. Notice that fast switching degrades very gracefully with elevation. Low elevation results are continued in the next Table.

ν [GHz]	t_{cal} [s]	t_{slew} [s]	S_{cal} [Jy]	distance [deg]	$vt/2 + d$ [m]	σ_ϕ [deg]	coherence eff.	duty eff.	total eff.
30 deg elevation									
37	0.040	0.95	0.046	0.58	165	23.3	0.921	0.925	0.852
81	0.056	1.01	0.067	0.67	153	29.4	0.877	0.925	0.811
113	0.069	0.98	0.064	0.62	127	36.6	0.815	0.894	0.729
157	0.101	1.06	0.086	0.79	130	31.7	0.858	0.894	0.767
209	0.137	1.12	0.107	0.92	147	29.2	0.878	0.894	0.785
271	0.172	1.12	0.113	0.95	133	29.7	0.874	0.894	0.782
355	0.182	1.19	0.150	1.07	135	29.1	0.879	0.894	0.786
415	0.241	1.24	0.172	1.18	160	28.0	0.887	0.925	0.821
650	0.323	1.31	0.207	1.40	133	28.9	0.881	0.894	0.787
20 deg elevation									
37	0.047	0.90	0.038	0.51	191	30.8	0.865	0.925	0.801
81	0.090	0.96	0.047	0.60	166	37.3	0.809	0.894	0.723
113	0.095	0.92	0.044	0.55	148	48.6	0.698	0.866	0.604
157	0.131	0.96	0.062	0.62	152	42.0	0.764	0.866	0.662
209	0.143	1.06	0.091	0.81	163	37.6	0.806	0.894	0.721
271	0.162	1.06	0.098	0.84	160	40.2	0.782	0.894	0.699
355	0.237	1.14	0.109	1.01	160	38.9	0.794	0.894	0.710
415	0.244	1.15	0.143	1.06	168	34.9	0.831	0.894	0.743
650	0.349	1.18	0.158	1.13	164	39.4	0.789	0.866	0.684

Table 3: Fast switching results: by matching the observing frequency to the atmospheric phase conditions and doing 400 Monte Carlo simulations of 90 GHz calibrator fields consistent with 90 GHz source counts, we optimize the switching strategy for each simulated observation and report the median efficiency. Notice that fast switching degrades very gracefully with elevation.

elevation [deg]	efficiency
80	0.859
60	0.853
45	0.833
30	0.783
20	0.692

Table 4: There is little degradation in mean efficiency (averaged over all frequency-matched phase conditions) as a function of elevation angle.

Holdaway, M.A., and J.R. Pardo, ALMA Memo 404, "Atmospheric Dispersion and Phase Calibration" 2001.

Holdaway, M.A., Satoki Matsushita, and M. Saito, "Preliminary Phase Stability Comparison of the Chajnantor and Pampa la Bola sites", ALMA Memo 176, 1997.

Holdaway, Owen, and Rupen, ALMA Memo 123, "Source Counts at 90 GHz", 1994.

Pardo, J.R., J. Cernicharo, and E. Serabyn "Atmospheric Transmission at Microwaves (ATM): An Improved Model for mm/submm applications" IEEE Trans. on Antennas and Propagation, accepted (Feb. 10, 2001).

Radford, S., "ALMA Site Web Page", 2001.

Robson, Yasmin, *et. al.*, ALMA Memo 345, "Phase Fluctuation at the ALMA Site and the Height of the Turbulent Layer", 2001.

Vertex Antennantechnique CDR, 2000.